Title: Coordinated IL-2 and TGF-β Signaling via a Novel Fusion Protein Selectively Expands and Activates Regulatory T Cells

One Sentence Summary

CUE-401 coordinates IL-2 and TGF-β signaling to expand and activate regulatory T cells and restrain autoimmune responses.

Authors

Nicholas M. Jackson[1], Javier A. Carrero[1], Kristin Yeung[2], Evelyn Needham[2], Emily Christie[2], Natalie Yakobian[1], Challen Pretorious[1], Stella Hoft[1], Kirsten Foley[1], Eric Ford[1], Simon Low[2], Ronald Seidel[2], Anish Suri[2], Natasha M. Girgis[2], Steven N. Quayle[2], Richard J. DiPaolo[1*]

[1]Department of Molecular Microbiology and Immunology, Saint Louis University School of Medicine, Saint Louis, Missouri

[2]CUE Biopharma, Boston, Massachusetts

Corresponding author, richard.dipaolo@health.slu.edu

Abstract

Safely and selectively re-establishing immune tolerance remains a central challenge in the treatment of autoimmune and inflammatory diseases. Regulatory T cells (Tregs) are essential mediators of immune homeostasis and peripheral tolerance. Interleukin-2 (IL-2) and transforming growth factor–β (TGF-β) synergize to promote Treg activation, differentiation, and stability, but coordinating selective in vivo delivery of these signals has limited potential therapeutic applications. Here, we describe CUE-401, a bifunctional biologic consisting of attenuated IL-2 and attenuated, receptor-masked TGF-β3 to promote co-signaling on target cells. In vitro, CUE-401 induced naïve $CD4^+$ T cells to convert to $Foxp3^+$ induced Tregs (iTregs), expanded endogenous Tregs, and suppressed inflammatory cytokine production by memory and effector $CD4^+$ T cells. In mice, a single dose of CUE-401 markedly increased the frequency of $CD4^+Foxp3^+$ Tregs exhibiting a stable and activated phenotype, with minimal activation of

27 $CD4^+Foxp3^-$ conventional T cells (Tconv) relative to an IL-2-only comparator. In a
28 Treg-deficiency-driven adoptive transfer model of autoimmunity, early administration of CUE-401
29 activated Tregs, reduced gastric infiltration by autoreactive T cells, and provided long-term protection
30 from autoimmune gastritis in the absence of continued treatment. Together, these findings support
31 CUE-401 as a dual IL-2/TGF-β3 biologic that promotes immune tolerance through coordinated induction,
32 expansion, and activation of Tregs while limiting activation of autoreactive $CD4^+$ T cells.
33

34 **Introduction**

35 Autoimmune diseases arise from the breakdown of peripheral immune tolerance, resulting in persistent
36 immune-mediated damage to self-tissues. The discovery of $CD4^+CD25^+$ regulatory T cells (Tregs)
37 marked a paradigm shift in understanding immune tolerance (*1*). Tregs maintain tolerance by suppressing
38 autoreactive effector T cell responses while preserving protective immunity through multiple
39 mechanisms, including consumption of interleukin-2 (IL-2), expression of inhibitory receptors (e.g.
40 CTLA-4), and production of immunoregulatory cytokines, such as transforming growth factor–β (TGF-β)
41 (*2*). The essential role of Tregs in immune homeostasis is underscored by the severe autoimmune
42 pathology observed in humans and mice with mutations in the transcription factor Foxp3, which is
43 required for Treg lineage commitment and stability (*3-6*).
44

45 Tregs are classically defined by expression of CD4, the high-affinity IL-2 receptor α-chain (CD25), and
46 Foxp3. This population includes thymus-derived natural Tregs (nTregs) and peripherally induced Tregs
47 (pTregs), which arise from conventional $CD4^+$ T cells in response to antigenic stimulation and cytokine
48 cues (*7, 8*). In vitro, naïve $CD4^+$ T cells stimulated with TCR signals plus TGF-β, and IL-2 differentiate
49 into $Foxp3^+$ induced Tregs (iTregs) with potent suppressive activity (*9*). Precise modulation of IL-2–
50 dependent STAT5 activation together with TGF-β–mediated Foxp3 induction is also critical for
51 maintaining stable, suppressive Tregs (*9-11*). Accordingly, this cytokine combination has been widely

52 used to generate suppressive iTregs ex vivo for adoptive cell therapies that are effective in preclinical
53 models of autoimmunity and graft-versus-host disease (*12-14*).
54
55 The immunosuppressive capacity of Tregs has motivated their therapeutic use in transplantation and
56 immune-mediated diseases. Several different IL-2 variants (muteins) have been engineered to activate and
57 expand Tregs and are being tested for effectiveness in treating inflammatory diseases (*15-17*). Key
58 challenges include a limited therapeutic window due to off-target stimulation of non-Treg populations, the
59 short half-life of IL-2, and the need for precise dosing to achieve selective Treg engagement. Moreover,
60 Treg induction, stability, and specialization in vivo often require additional cues, including TGF-β.
61 Coordinating IL-2 and TGF-β signaling in vivo is challenging due to short in vivo half-lives of cytokines,
62 tolerability considerations, and the need to co-engage receptors on the same target cell(s). CUE-401, a
63 novel Fc-based IL-2/TGF-β3 fusion protein designed for coordinated delivery of IL-2 and TGF-β signals
64 in vivo, was designed to address these challenges. CUE-401 includes an attenuated IL-2 mutein (F42A,
65 H16A) with reduced affinity for CD25 and CD122 (*18-20*), and a novel receptor-masked attenuated TGF-
66 β3 variant, linked via flexible linkers to an Fc scaffold to promote IL-2/TGF-β3 co-signaling and extend
67 half-life. All amino acid sequences are human-derived, and both cytokines cross-react with mouse
68 receptors (*21, 22*). Here, we evaluated the biological activities of CUE-401 in vitro and in vivo for its
69 ability to enhance Tregs, suppress effector T cell responses, and mitigate autoimmune pathology.
70
71 **Results**
72
73 **CUE-401 delivers IL-2 and TGF-β signals to T cells**
74 CUE-401 is a bispecific fusion protein composed of affinity attenuated variants of IL-2 and TGF-β3 (Fig.
75 1A). The IL-2 mutein (F42A and H16A) reduces affinity to IL-2Rα (CD25) and IL-2Rβ (CD122) (*18*). The
76 TGF-β3 component is engineered as a monomeric, receptor masked variant to enhance manufacturability
77 and attenuate receptor affinity. The TGF-β3 moiety in CUE-401 carries a C77S mutation that prevents

78 formation of the interchain disulfide bond while maintaining its ability to assemble the natural signaling
79 complex. The masking component consists of a modified TGFβR2 extracellular domain lacking the
80 N-terminal 25 amino acids required for TGFβR1 interaction and incorporating an D118A mutation to
81 reduce affinity for TGF-β3 relative to the wild-type receptor (*23, 24*). This masked configuration preserves
82 biological activity but enables CUE-401 to be manufactured at scale in soluble form and subsequently
83 activated upon engagement at the cell surface. Both cytokine domains are connected via flexible linkers to
84 a heterodimeric Fc scaffold to promote co-signaling, enhance molecular stability, extend serum half-life.
85
86 The IL-2 activity of the CUE-401 molecule was quantified using CTLL-2 proliferation assays. Three
87 conditions were tested: 1. wild-type human IL-2 (Proleukin), 2. CUE-401, and 3. A version of CUE-401
88 that contains the IL-2 mutein (F42A and H16A) but is lacking a TGF-β3 (referred to as CUE-401ΔTGFβ;
89 Fig. 1B). Both CUE-401 and CUE-401ΔTGFβ induced dose-dependent proliferation that was attenuated
90 compared to Proleukin (Fig. 1B). TGF-β3 activity of CUE-401 was demonstrated by SMAD2/3
91 phosphorylation in murine splenocytes treated with CUE-401 or recombinant TGF-β3, but not with rIL-2
92 alone, or in cells that were pretreated with a selective inhibitor of TGF-βR signaling, SB431542 (Fig. 1C).
93
94 **CUE-401 induces and expands Tregs and suppresses effector T cell function in vitro**
95 After confirming that both cytokine components of CUE-401 were biologically active, we determined
96 whether CUE-401 could induce de novo Foxp3 expression in $CD4^+$ T cells. $CD4^+CD8^-$Foxp3.GFP^- thymic
97 T cells were sorted from thymi of BALB/c.Foxp3.eGFP mice and stimulated with anti-CD3/anti-CD28 in
98 the presence of recombinant human IL-2 (rhIL-2), rhIL-2 plus recombinant human TGF-β3 (rhTGF-β3), or
99 CUE-401 (Fig. 2). IL-2 alone induced minimal Foxp3 expression (~1%), whereas both rhIL-2 + rhTGF-β3,
100 and CUE-401 induced Foxp3 expression in >75% of $CD4^+$ T cells (Fig. 2A). CUE-401 induced Foxp3
101 expression in a dose-dependent manner, with an EC_{50} of ~18 nM (Fig. 2B). These data demonstrate that
102 CUE-401 is effective at co-delivering IL-2/TGF-β signals required for $Foxp3^+$ iTreg induction from naïve
103 CD4 T cells.

104

105 To assess whether CUE-401 expands endogenous $CD4^+Foxp3^+$ Tregs, $CD4^+Foxp3.eGFP^+$ Tregs sorted
106 from the spleens of BALB/c.Foxp3.eGFP mice were stimulated with anti-CD3/anti-CD28 in the presence
107 of either rhIL-2 (control) or CUE-401. As expected, Tregs maintained Foxp3 expression when cultured
108 with rhIL-2 (Fig. 2C). Similarly, Tregs stimulated in the presence of CUE-401 also maintained Foxp3
109 expression and expanded in a dose-dependent manner (Fig. 2D). These results demonstrate that CUE-401
110 effectively promotes Treg maintenance and expansion in vitro.

111

112 To determine the effects of CUE-401 on effector/memory T cells, $CD4^+CD44^{hi}Foxp3.eGFP^-$ cells sorted
113 from spleens of BALB/c.Foxp3.eGFP mice were stimulated with anti-CD3/anti-CD28 in the presence of
114 either rhIL-2, rhIL-2 + rhTGF-β3, or CUE-401 (Fig. 2E). Treatment with rhIL-2 resulted in minimal
115 induction of Foxp3 expression (~1%). However, stimulation of these purified effector/memory T cells in
116 the presence of rhIL-2 + rhTGF-β3 or CUE-401 induced Foxp3 expression in ~10% of effector/memory
117 $CD4^+$ T cells (Fig. 2E-F). Next, we assessed cytokine secretion by effector/memory $CD4^+$ T cells from
118 these same cultures. In the presence of IL-2, effector/memory T cells secreted IFN-γ, IL-4, TNF, and IL-
119 17A. However, CUE-401 significantly decreased the secretion of IFN-γ, IL-4 and TNF from these
120 stimulated effector cells compared to rhIL-2 alone (Fig. 2G). Together, these findings establish three key
121 biological activities of CUE-401 in vitro: (1) induction of iTregs from naïve $CD4^+$ T cells, (2) maintenance
122 of Foxp3 expression and expansion of existing Tregs, and (3) induction of Foxp3 expression in a subset
123 and reduced proinflammatory cytokine production by effector/memory $CD4^+$ T cells.

124

125 **CUE-401 administration induces robust expansion of stable regulatory T cells in mice**

126 To evaluate the biological activities of CUE-401 in vivo, BALB/c mice received a single dose of CUE-401
127 or vehicle (PBS). By day 6, Treg frequencies in the spleen of CUE-401 treated mice increased to ~61% of
128 $CD4^+$ T cells compared to ~20% in controls (Fig. 3A-B). To characterize the phenotype and stability of
129 Tregs expanded by CUE-401 in vivo, we assessed methylation of the Treg-specific demethylated region

130 (TSDR), a CpG-rich enhancer within the *Foxp3* locus (CNS2) (*25*). Splenocytes from vehicle and CUE-
131 401 treated mice were sorted to be $CD4^+$Foxp3.$eGFP^+$ and $CD4^+$Foxp3.$eGFP^-$ (Fig. 3C). Tregs from CUE-
132 401-treated mice exhibited comparable demethylation of the TSDR to that observed in natural Tregs in
133 control mice, whereas the TSDR in Tconv cells from CUE-401 treated mice was similarly methylated as in
134 natural Tconv cells from untreated animals (Fig. 3D). Furthermore, Tregs from both groups maintained
135 stable Foxp3 expression after restimulation for 6 days in vitro in the absence of further treatment (Fig. 3E).
136 These findings demonstrate that CUE-401 expands stable, lineage-committed Tregs in vivo.
137

138 **Expanded regulatory T cells exhibit an activated phenotype following CUE-401 administration**

139 After establishing that CUE-401 administration induced a robust expansion of Tregs, we next compared
140 Treg phenotypes between treated and control mice 6 days after treatment. As shown above, CUE-401
141 significantly increased the frequency of $CD4^+$Foxp3^+ Tregs compared with PBS-treated controls (Fig. 4A).
142 These Tregs were then analyzed for expression of markers of Treg activation and suppressor functions (*26,*
143 *27*), including Foxp3, GITR, CD25, CTLA-4, CD103, CD73, CD38, CD134, CD137, and Ki67. Flow
144 cytometry and UMAP analysis identified enrichment of activated Treg clusters in CUE-401–treated mice,
145 with increased frequencies of $GITR^{hi}$/$CD25^{hi}$ and CTLA-4^{hi}/$CD103^{hi}$ Tregs, and higher expression of
146 CD25, CTLA-4, and GITR overall (Fig. 4A–C).
147

148 To gain deeper insight into the effects of administering CUE-401 on Tregs, we compared gene expression
149 profiles on Tregs from CUE-401 treated and control mice (Fig. 4D). Bulk RNA-seq of purified Tregs
150 revealed upregulation of several genes associated with Treg activation and suppressive function in CUE-
151 401 treated mice, including *Itgae* (CD103), *Nrp1* (neuropilin-1), *Il2ra* (CD25), *Il2rb* (IL-2Rβ), *Lag3* (LAG-
152 3), *Tnfrsf18* (GITR), *Icosl* (ICOSL), and *Klrg1* (KLRG1) (*28-32*). Together, these data demonstrate that
153 CUE-401 not only expands a stable Treg population in vivo but also promotes a transcriptional program
154 associated with enhanced activation and suppressive capacity (*33-36*).
155

156 **Combined IL-2 and TGF-β signaling responses in Tregs are distinct from IL-2 alone**

157 To dissect the contribution of TGF-β3 and to compare the biological activity of CUE-401 to a biologic that
158 delivers only IL-2, we compared CUE-401 to CUE-401ΔTGF-β3, which contain the identical variant of
159 IL-2. In vivo, both molecules induced significant expansion of splenic Tregs, although Treg frequencies
160 were higher in CUE-401-treated mice (Fig. 5A, B). CUE-401 also increased the proportion of GITR^{hi}
161 CD38^{hi} Tregs more than CUE-401ΔTGF-β3 did (Fig. 5C, D). Furthermore, the IL-2–only version increased
162 CD25 and CD103 expression on Tconv, whereas the TGF-β3-containing CUE-401 did not (Fig. 5E–F).

163

164 Transcriptomic analyses of sorted CD4^{+}Foxp3.GFP^{+} Tregs and CD4^{+}Foxp3.GFP^{-} Tconv from PBS,
165 CUE-401ΔTGF-β3, and CUE-401 treated mice also revealed different biological activities of IL-2 in the
166 presence or absence of TGF-β3 signaling. Both CUE-401ΔTGF-β3 and CUE-401 increased the expression
167 of core Treg-associated genes, including: *Ctla4*, *Foxp3*, *Il2ra*, and *Lag3*, relative to PBS-treated controls
168 (Fig. 5G). However, several of the IL-2 induced genes induced in Tregs by the IL-2 only version
169 (CUE-401ΔTGF-β3) were not induced following treatment with CUE-401 (i.e. IL-2 and TGF-β3).
170 Furthermore, a subset of transcripts known to be regulated by TGF-β, including *Alpk1*, *Amot1*, *Cyp4f18*,
171 *Lgmn*, and *Trim47*, were specifically induced in Tregs treated with CUE-401 and not with
172 CUE-401ΔTGF-β3. Together, these findings demonstrate that co-delivery of IL-2 and TGF-β3 by CUE-
173 401 promotes a Treg-specific transcriptional state that is distinct from, and not simply an amplification of,
174 the program induced by IL-2 alone.

175

176 Conversely, within the CD4^{+}Foxp3^{-} Tconv population, treatment with CUE-401ΔTGF-β3 induced a
177 transcriptional program characteristic of IL-2–driven cellular activation, including *Ccl4, Eomes, Fut7,*
178 *GzmA, Gzmb, Lgals1, Lgals3, Ly6a, Morrbid, Nfil3, S100a6*, which were not increased in Tconv of CUE-
179 401–treated mice (Fig. 5H). Together, these data show that the IL-2 component of CUE-401 can activate
180 Tconv, but that this IL-2 induced Tconv activation does not occur following co-delivery with TGF-β3.

181 Thus, CUE-401 elicits distinct responses in Tregs compared to IL-2 alone and exhibits greater selectivity
182 for Treg responses compared to Tconv.
183
184 **Early administration of CUE-401 ameliorates autoimmune gastritis.**
185 To evaluate the therapeutic effects of CUE-401 in autoimmunity, we used a well-established mouse model
186 of Treg-deficiency–driven autoimmune gastritis, in which $CD25^+$ cells (Tregs) are depleted from BALB/c
187 splenocytes and transferred into athymic BALB/c *nu/nu* recipients (*1*). Severe Treg loss in the transferred
188 population reliably induces autoimmune gastritis in 100% of recipients. To facilitate tracking of antigen-
189 specific autoreactive Tconv cells in this system, a small number of $CD4^+$ TCR-transgenic Tconv cells
190 specific for the gastric autoantigen H^+/K^+ ATPase (*37*) and expressing the Thy1.1 congenic marker were
191 mixed with CD25-depleted BALB/c splenocytes ($Thy1.2^+$) prior to transfer. Figure 6A shows a
192 representative flow cytometry plot of CD4-gated T cells before transfer, illustrating the CD25-depleted
193 BALB/c splenocytes ($Thy1.2^+$) mixed with autoreactive transgenic T cells ($Thy1.1^+$).
194
195 Recipient BALB/c *nu/nu* mice were dosed on days 1 and 14 with PBS or CUE-401. At day 62, the frequency
196 of autoreactive H^+/K^+ ATPase-specific $CD4^+Thy1.1^+$ T cells infiltrating the gastric mucosa was
197 significantly lower in CUE-401–treated mice compared to PBS treated mice (approximately 10% versus
198 44%; $P = 0.0005$; Fig. 6B, C). Stomachs were also processed for histopathological analysis to assess disease
199 severity, including inflammation, glandular atrophy, and hyperplasia, three hallmark features of
200 autoimmune gastritis (*38*). As expected, control mice developed moderate-to-severe autoimmune gastritis,
201 with a median disease score of 6 out of 12. In contrast, disease severity was significantly reduced in CUE-
202 401–treated mice, with a median pathology score of 3 out of 12, with three mice exhibiting no detectable
203 disease (Fig. 6D, E). Together, these results demonstrate that early and transient administration of CUE-
204 401 conferred durable suppression of auto-reactive T cells, as well as protection against autoimmune
205 gastritis–associated pathology in a well-established model of Treg deficiency–driven autoimmunity.
206

207 **CUE-401 treatment induces a distinct regulatory T cell phenotype in a disease setting**

208 To investigate the mechanism(s) by which the administration of CUE-401 suppressed autoimmune gastritis
209 in this model we analyzed the immune cells in PBS and CUE-401 mice using flow cytometry and single
210 cell RNA sequencing on cells isolated from gastric lymph nodes and spleens seven days after cell transfer
211 (six days after a single administration of PBS or CUE-401). Treg frequency in stomach draining lymph
212 nodes was significantly increased in CUE-401–treated mice (~25%) compared with PBS-treated controls
213 (~10%) (Fig. 7A, B). To further compare Treg phenotypes, we gated on $CD4^{+}Foxp3^{+}$ Tregs and performed
214 high-dimensional flow cytometry analysis, applying unsupervised dimensionality reduction with Uniform
215 Manifold Approximation and Projection (UMAP) of expression of Foxp3, GITR, CD25, CTLA-4, CD103,
216 CD73, CD38, CD134, CD137, and Ki67. UMAP projections revealed distinct clustering of Tregs from PBS
217 versus CUE-401 treated mice, indicating differential protein expression profiles between treatment groups
218 (Fig. 7C). Among these, CD25 expression was higher on Tregs from CUE-401 treated mice compared with
219 PBS controls (Fig. 7D). These data demonstrate that CUE-401 both increases the frequency of Tregs and
220 enhances expression of activation-associated receptors such as CD25 in this disease model.

221

222 To further define the effects of CUE-401 on the Treg phenotype and transcriptional state, we performed
223 single-cell RNA sequencing on cells isolated from gastric lymph nodes and spleens seven days after cell
224 transfer (six days after a single administration of PBS or CUE-401). $Foxp3^{+}$ Tregs formed a unique UMAP
225 cluster in each treatment condition (Fig. 7F). $Foxp3^{+}$ cells were isolated for downstream analysis, and gene
226 set enrichment revealed that Tregs from CUE-401–treated mice were significantly enriched for higher
227 expression of IL-2/STAT5 signaling signature transcripts compared with Tregs from PBS-treated mice
228 (Fig. 7G).

229

230 Consistent with this observation, a heatmap highlighting differentially expressed genes demonstrated
231 increased expression of transcripts associated with Treg activation, suppressive function, and survival in
232 CUE-401–treated mice, including *Il2ra* (CD25), *Tnfrsf4* (OX40), *Tnfrsf9* (4-1BB), *Tnfsf11* (RANKL),

233 *Il1rl1* (ST2), and *Bcl2l1* (BCL-xL) relative to PBS-treated mice (Fig. 7H). Together, these data demonstrate
234 that administration of CUE-401 following transfer of Treg-depleted splenocytes increases Treg abundance
235 and induces a distinct transcriptional program in Tregs that is associated with activation and suppressive
236 activities, providing mechanistic insight into the early immunological effects of CUE-401 that contribute
237 to long-term protection from autoimmune disease.
238
239 **Discussion**
240 CUE-401 is a novel bifunctional Fc–IL-2/TGF-β3 fusion protein that enables coordinated cytokine delivery
241 to selectively promote Treg induction, expansion, and activation. In vitro, CUE-401 efficiently generated
242 induced Tregs (iTregs), expanded endogenous Tregs, and enhanced Foxp3 expression while suppressing
243 cytokine production in effector and memory T cells, which are effects consistent with integrated IL-2 and
244 TGF-β3 signaling. In vivo, CUE-401 increased Treg frequency and activation while limiting Tconv
245 activation relative to IL-2 alone, and ameliorated disease in a Treg-deficiency–driven gastritis model.
246 Transcriptomic analyses further indicate that CUE-401 elicits a Treg program that is qualitatively distinct
247 from that induced by IL-2 monotherapy, and while IL-2 alone activates Tconv, the IL-2 and TGF-β3
248 together in CUE-401 did not activate Tconv, speaking to an opportunity for enhanced Treg selectivity with
249 this approach. While additional studies will be required to more fully assess these responses in additional
250 chronic disease settings, the current data supports robust short-term Treg reprogramming in vivo and long-
251 term prevention of autoimmunity.
252
253 Prior studies established that iTregs generated ex vivo with IL-2 and TGF-β can suppress autoimmunity
254 following adoptive transfer (*33-36, 39, 40*). However, these approaches required cell manufacturing and
255 did not directly address whether coordinated cytokine delivery can be achieved pharmacologically in vivo.
256 Our findings demonstrate that CUE-401 enables such coordination, promoting Treg expansion and
257 activation without broadly stimulating conventional T cells. Notably, CUE-401 induced an activated Treg
258 phenotype while minimizing activation of Foxp3^{-} Tconv, an effect not observed with an IL-2–only variant,

259 supporting the premise that linked IL-2 and TGF-β signaling preferentially biases responses toward the
260 Treg lineage. Future studies dissecting receptor-proximal signaling dynamics and cell-type–specific
261 cytokine engagement will further refine this model (*41*).
262
263 At the molecular level, Tregs treated with CUE-401 exhibited durable Foxp3 expression, demethylation of
264 the Foxp3 TSDR, and sustained Foxp3 maintenance upon restimulation, features associated with lineage
265 stability. These properties are particularly important given the reported instability of some iTreg
266 populations under inflammatory conditions (*42-45*). Although overall Treg frequencies normalized to
267 baseline levels after ~14 days (data not shown), CUE-401 expanded cells maintained a stable Foxp3^{+}
268 phenotype in both homeostatic and inflammatory settings, consistent with physiological regulation of the
269 compartment rather than loss of lineage identity. Longer-term lineage-tracing studies will be valuable to
270 definitively distinguish de novo induction from selective expansion in vivo.
271
272 Mechanistically, CUE-401 drove coordinated activation of CD25/IL-2/STAT5 pathways while avoiding
273 induction of effector-like programs. Studies with a TGF-β–deficient variant (CUEΔTGF-β3) established
274 that TGF-β3 is required for selective Treg activation and for constraining off-target CD4^{+} Tconv responses,
275 supporting a TGF-β–dependent mechanism of action. Together, these data indicate that physically linked
276 cytokine co-delivery can reshape IL-2 responsiveness toward a regulatory-biased state. Whether this
277 reflects altered cytokine receptor geometry, local concentration effects, or cooperative signaling remains
278 an important question for future mechanistic studies.
279
280 Collectively, our findings position CUE-401 as a modular strategy for in vivo Treg programming that may
281 overcome key limitations of current IL-2–based therapies. By promoting expansion and activation of stable,
282 lineage-committed Tregs while minimizing effector T cell activation, CUE-401 represents a promising
283 therapeutic approach for autoimmune and inflammatory diseases. Evaluation in additional disease models
284 and human systems will be important next steps toward clinical translation.

285

286 **Materials and Methods**

287

288 **Study design**

289 The objective of this research was to define the activities of a new biologic that co-engages IL-2 and TGF-
290 β pathways on regulatory T cells. This was accomplished by experimentally testing the function of the
291 biologic, named CUE-401, in vitro and in vivo. In vitro, testing was performed to address the induction of
292 iTregs from naïve $CD4^+$ T cells, maintenance of Foxp3 expression and expansion of existing Tregs, and
293 induction of Foxp3 expression with reduced proinflammatory cytokine production in a subset of
294 effector/memory $CD4^+$ T cells. CUE-401 was also administered to mice. Expression of Foxp3 and other
295 activation related proteins were measured by flow cytometry and compared by uniform manifold
296 approximation and projection analysis. Stability of in vivo Tregs was assessed by measuring the
297 methylation state of CpG sites in the Treg specific demethylated region, and $Foxp3^+$ cells were restimulated
298 to verify maintenance of Foxp3 expression. CUE-401's ability to affect disease severity was measured
299 through tracking autoreactive T cells, pathological scores of disease in the stomachs of an established mouse
300 model of autoimmunity. Single cell RNA sequencing was done to address potential mechanisms of action
301 for disease.

302

303 **CUE-401 design and production**

304 CUE-401 was produced by transient transfection of ExpiCHO-S cells using the Gibco ExpiCHO Expression
305 System Max Titer Protocol. Each transfection is performed with two plasmids at a 1:1 molar ratio encoding
306 (1) IL2 mutein linked to human IgG1Fc (knob) linked to monomeric TGFß3 and (2) human IgG1Fc (hole)
307 linked to truncated TGFßR2, respectively. Upon harvest, conditioned media was loaded onto a mAb Select
308 SuRe protein A column using an AKTA Pure 25 system for affinity-based purification. After a 10-column
309 volume (cv) wash with 20mM HEPES pH 7.5 + 1M NaCl, CUE-401 was eluted using 50mM glycine pH
310 2.8 directly into 10% 1M Tris pH 9.0 neutralization solution. Eluant was pooled, concentrated and loaded

311 onto a HiLoad 26/600 Superdex 200 for final step purification by size exclusion chromatography in 1x PBS
312 pH 7.4. Main protein elution peak was collected, pooled, concentrated, filtered using a 2um syringe filter.
313 Protein concentration was measured by absorbance at 280nm (A_{280}) using a NanoDrop system. Protein
314 integrity, size, solution state, and purity were confirmed by liquid chromatography-mass spectrometry,
315 SDS-PAGE, and analytical size exclusion chromatography. Final purified protein was aliquoted and stored
316 at -80ºC until use.
317
318 **Mice**
319 Female BALB/c Thy1.1^{+} mice were bred in house and BALB/c *nu/nu* (4–8 wk old) were purchased from
320 the Charles River Laboratory and housed under specific pathogen-free conditions. TCR transgenic mice
321 were crossed with BALB/c Thy1.1/1.1 expressing mice as previously described (*37*). TCR Transgenic
322 Thy1.1/1.1 expressing mice that develop autoimmune gastritis were crossed with BALB/c Thy1.1/1.1
323 Foxp3.eGFP reporter mice (C.Cg-*Foxp3*^{tm2Tch}/J) to generate TCR transgenic Thy1.1/1.1 Foxp3.eGFP
324 reporter mice (*42*). All animals were maintained in the Department of Comparative Medicine, Saint Louis
325 University School of Medicine in accordance with institutional guidelines (Association for Assessment and
326 Accreditation of Laboratory Animal Care, International accreditation number 000656).
327
328 **CUE-401 Dosing**
329 CUE-401 was formulated in sterile PBS, pH 7.4. Mice received intraperitoneal (i.p.) injections of CUE-401
330 at 2 mg/kg (100 µg/mL; 10 mL/kg; typical injection volume ~0.2–0.3 mL per 20–30 g mouse) or PBS
331 (vehicle) on the indicated schedule. For the adoptive transfer model, dosing occurred on days +1 and +14
332 post-transfer. For pharmacodynamic studies of Treg expansion, a single dose was administered, and tissues
333 were analyzed on day 6.
334
335 **CTLL-2 proliferation assays**

336 CTLL-2 cells were cultured in RPMI 1640 medium (Thermo Fisher Scientific, Waltham, MA, USA)
337 supplemented with 10% heat-inactivated fetal bovine serum (Thermo Fisher Scientific, Waltham, MA,
338 USA) and were starved of IL-2 for 22–24 h by washing cells free of cytokine and incubating them at
339 1×10^5 cells/mL in IL-2–free medium at 37°C with 5% CO_2. Cell viability and morphology were assessed
340 before and after starvation via acridine orange/propidium iodide staining using a Cellaca MX automated
341 cell counter (Nexcelom Bioscience, Lawrence, MA, USA). On the day of assay, 5×10^3 viable CTLL-2
342 cells were seeded in 96-well tissue-culture-treated plates (Corning/Costar, Corning, NY, USA) in 100 µL
343 medium, with outer wells filled with DPBS (Thermo Fisher Scientific, Waltham, MA, USA) to minimize
344 edge effects. Test molecules and recombinant rhIL-2 were prepared at 2× concentration and added in 100
345 µL to achieve a final volume of 200 µL per well, with all conditions plated in triplicate. After 72 h
346 incubation at 37°C, cell viability was quantified using CellTiter-Glo® reagent (Promega, Madison, WI,
347 USA): plates were equilibrated to room temperature, 100 µL of suspension was transferred to white
348 flat-bottom 96-well assay plates (Corning/Costar, Corning, NY, USA), an equal volume of CellTiter-Glo
349 was added via reverse pipetting, plates were agitated and incubated for 10 min, and luminescence was
350 measured using a Synergy Neo2 multimode plate reader (BioTek Instruments, Winooski, VT, USA).
351

352 **pSMAD Detection**

353 Murine splenocytes and human PBMCs were used to evaluate pSMAD2 signaling in response to
354 CUE-401 stimulation and TGF-β pathway inhibition. Fresh spleens from BALB/c mice were processed
355 through a 0.7-µm strainer to obtain single-cell suspensions, followed by ACK lysis, washing in PBS, and
356 counting on a Cellaca MX automated cell counter. Cells were aliquoted at 5×10^7 per condition and rested
357 for 2 h at 37°C, with subsets pre-treated for 90 min with 10 µM TGF-β inhibitor. PBMCs were thawed
358 and washed similarly. Cells were treated for 30 min at 37°C with IL-2, TGF-β3, CUE-401, or
359 combinations thereof, and then washed and lysed with RIPA buffer (Thermo Fisher Scientific, Waltham,
360 MA, USA) supplemented with Halt Protease/Phosphatase Inhibitor Cocktail (Thermo Fisher Scientific,
361 Waltham, MA, USA). Lysates were homogenized by pipetting, clarified by centrifugation at 10,000 rpm

362 for 10 min at 4°C, and protein content was quantified using a BCA assay. Samples were mixed with LDS
363 loading buffer (Thermo Fisher Scientific, Waltham, MA, USA), heated, and resolved on Bolt 4–12%
364 Bis-Tris Plus polyacrylamide gels (Thermo Fisher Scientific, Waltham, MA, USA) alongside SeeBlue
365 Plus Prestained Standards (Thermo Fisher Scientific, Waltham, MA, USA). Following electrophoresis,
366 proteins were transferred to PVDF membranes using the iBlot 2 Dry Blotting System (Thermo Fisher
367 Scientific, Waltham, MA, USA), then blocked for 2 h at room temperature in SuperBlock buffer (Thermo
368 Fisher Scientific, Waltham, MA, USA). Membranes were incubated overnight at 4°C with primary
369 monoclonal antibodies against phospho-SMAD2 (Cell Signaling Technology, Danvers, MA, USA) or
370 total SMAD2/3 (Cell Signaling Technology, Danvers, MA, USA). After washing, membranes were
371 incubated with HRP-conjugated goat anti-rabbit IgG (Cell Signaling Technology, Danvers, MA, USA)
372 for 1 h at room temperature, washed again, and developed using SuperSignal West Femto or West Pico
373 chemiluminescent substrates (Thermo Fisher Scientific, Waltham, MA, USA). Western blots were
374 imaged using a Syngene G:BOX darkroom imaging system (Syngene, Frederick, MD, USA). Band
375 intensities were analyzed to quantify pSMAD2 induction and inhibition across treatment conditions.
376

377 **Isolation of Immune Cells**

378 Isolation of immune cells from stomach tissue has been described previously (*38, 43*). Briefly, stomachs
379 were harvested from mice, gastric lymph nodes were removed, and the stomachs were dissected along the
380 lesser curvature. Stomachs were rinsed with cold PBS then injected with 10 mL of cold MACS buffer (1 x
381 PBS,0.5% BSA (Fisher Scientific Waltham, MA), 2 mM EDTA (Promega, Fitchburg, Wisconsin)) using a
382 27-gauge needle, to inflate the tissue and free infiltrating immune cells. After injection, the stomach was
383 diced and collected with the 10mL of MACS buffer and transferred to a 50 mL conical tube. The dispersed
384 stomach tissue was mixed thoroughly then passed through a 40-micron filter, washed with 40 mL of MACS
385 buffer and used for analysis. Immune cells from the spleen and gastric/pancreatic lymph node were
386 processed by dispersing on a 40-micron filter and washed with 15 mL of MACS buffer. Spleen cells were
387 spun down at 2000 RPM for 5 minutes after initial processing. Spleen cells were resuspended in 5 mL of

388 1x ACK lysis buffer (Thermo Fisher Scientific, Waltham, MA) for 10 seconds then washed with 45 mL of
389 MACS buffer and spun again at 2000 RPM for 5 minutes. Cells were resuspended and filtered again through
390 a 40-micron filter before being counted and utilized for experiments.
391

392 **T cell purification, iTreg differentiation, and nTreg expansion**

393 Inducible Tregs (iTreg) were generated as previously described (*9*). Briefly, $CD4^{+}CD8^{-}$ thymocytes or
394 $CD4^{+}$Foxp3.eGFP^{+} splenocytes were sorted from 6-8-wk-old BALB/c mice and stimulated with plate-
395 bound anti-CD3 (1 mg/ml) and anti-CD28 (2 mg/ml; BD Biosciences) in 24-well plates ($2.5x10^{5}$ cells/well)
396 in 2 ml RPMI media (modified RPMI 1640 (Corning, Tewksbury, Massachusetts) supplemented with 10%
397 fetal bovine serum (FBS; Biotechne, Minneapolis, Minnesota), 2 mM glutamine (Sigma-Aldrich), 100 U/ml
398 penicillin,100 mg/ml streptomycin (Sigma-Aldrich), 10 mM HEPES (Sigma-Aldrich), β-mercaptoethanol
399 (55mM), 1 mM essential amino acids (Gibco, Billings, Montana), and 1 mM sodium pyruvate (Sigma-
400 Aldrich) supplemented with recombinant human IL-2(rhIL-2) (National Institutes of Health, Bethesda,
401 Maryland) (100 U/ml). Recombinant human TGF-β3 (rhTGF-β3) (Biotechne) (5 ng/ml) was added to
402 induce iTregs. Cells were removed from plate-bound antibodies after 48 hours and added to new wells with
403 fresh media supplemented with 100 U/ml recombinant human IL-2. Cells were used after 7 days in culture.
404 Endogenous Treg expansion was assessed by isolating FACS-purified splenic $CD4^{+}$Foxp3.eGFP^{+} Tregs.
405 Tregs were stimulated with plate-bound anti-CD3 & anti-CD28 and expanded with IL-2 (100 U/mL) or
406 CUE-401 as indicated for 5–7 days. Foxp3 maintenance and cell counts were assessed by flow cytometry.
407

408 **Effector/Memory $CD4^{+}$ T-Cell Restimulation and Cytokine Quantification**

409 Splenic $CD4^{+}CD44^{hi}$ Foxp3.eGFP^{-} T cells were FACS-sorted and stimulated with plate-bound anti-CD3 &
410 anti-CD28 in the presence of rhIL-2 (100 U/mL), rhIL-2 + rhTGF-β3 (5 ng/mL), or CUE-401. For cytokine
411 secretion, cells were cultured at 1×10^{6} cells/mL and restimulated with 25ng/mL phorbol myristate acetate
412 (PMA) (Sigma-Aldrich, St. Louis, Missouri), and 500 ng/mL ionomycin (Sigma-Aldrich), for 72 hours at
413 37°C for 72 h. Supernatants were collected and cytokine secretion was analyzed using a Th1, Th2, Th17

414 and IL-13 flex set (BD Biosciences) cytometric bead array kit and analyzed by flow cytometry following
415 the kit protocol and analyzed by flow cytometry.
416
417 **Treg Stability: TSDR (CNS2) Methylation Analysis**
418 $CD4^+Foxp3^+$ and $CD4^+Foxp3^-$ cells were sorted from spleens of PBS- or CUE-401-treated mice 6 days
419 post-dose. Genomic DNA was isolated (DNeasy Blood & Tissue Kit, Qiagen), bisulfite-converted (EZ
420 DNA Methylation-Gold Kit, Zymo Research), and the Foxp3 TSDR (CNS2) region was PCR-amplified
421 using validated primers spanning CpG sites within the enhancer. Amplicons were analyzed by
422 pyrosequencing [or Sanger sequencing of cloned products] to quantify methylation at individual CpGs.
423 Percent demethylation was calculated per CpG and averaged across the TSDR. Males and female mice
424 were used for TSDR analyses. Methylation state was normalized in female mice to account for the X-linked
425 Foxp3 locus inactivation in females.
426
427 **Bulk RNA-seq (Tregs and Tconv)**
428 $CD4^+Foxp3.eGFP^+$ regulatory T cells (Tregs) and $CD4^+Foxp3.eGFP^-$ conventional T cells (Tconv) were
429 FACS-sorted from spleens of PBS-, CUE-401–, or CUE-401ΔTGF-β3–treated BALB/c mice 6 days after
430 treatment (≥95% purity). Sorted cells were pelleted and immediately lysed in lysis buffer supplied with the
431 PureLink™ RNA Micro Kit (Invitrogen, Thermo Fisher Scientific), and total RNA was extracted according
432 to the manufacturer's protocol. RNA was eluted in RNase-free water and quantified using a Qubit RNA HS
433 Assay (Thermo Fisher). RNA integrity was assessed using the Agilent Bioanalyzer RNA Pico Kit, and only
434 samples with RIN ≥7.0 were used for library preparation.
435 Libraries were generated using the Takara-Clontech SMARTer construction method for Illumina with
436 poly-A mRNA enrichment, following manufacturer instructions. Indexed libraries were pooled and
437 sequenced on an Illumina NovaSeq x Pluse (300 cycles) platform (paired-end 2×100 bp), targeting ≥30
438 million read pairs per sample.

439 Samples were processed and sequenced at the Genome Technology Access Center @ McDonnell Genome
440 Institute in St. Louis, Missouri. RNA-seq reads were then aligned to the Ensembl GRCm39.113 primary
441 assembly with STAR version 2.7.11b. Gene counts were derived from the number of uniquely aligned
442 fragments by Subread:featureCount version 2.0.8. Differential gene expression analysis was performed
443 with EdgeR using quasi-likelihood F-test and was adjusted using the Benjamini-Hochberg method. Genes
444 with a false discovery rate (FDR) < 0.05 were considered significantly differentially expressed and adjusted
445 *P* value was $p < 0.05$. Level counts were obtained with featureCount. Visualization of the heatmaps was
446 generated using the R package pheatmap. Level counts were obtained with featureCounts. Differential gene
447 expression analyses were performed using DESeq2. Significance thresholds were set at an adjusted
448

449 **Cell purification and injection for adoptive transfer model of autoimmune gastritis**

450 Naive TxA23 T cells were isolated from a single-cell suspension of thymii from TxA23.Thy-1.1
451 Foxp3.eGFP mice. Thymocytes were lysed with ACK lysis buffer (BioSource) and washed with MACS
452 buffer prior to staining with CD4 BV421 (BD Biosciences) and CD8 PE (BD Biosciences). Cells were
453 placed in FACS sort buffer (2% FBS (Biotechne, Minneapolis, Minnesota), 100 U/ml penicillin, 100 mg/ml
454 streptomycin, in complete RPMI without phenol red (Sigma-Aldrich), and then purified using the BD
455 FACSAria Fusion cell sorter (BD Biosciences) to obtain $CD4^+CD8^-$ GFP^- Cells. BALB/c Splenocytes were
456 from spleens of healthy Thy-1.2 expressing BALB/c mice, RBC were removed with ACK lysis buffer and
457 then purified as follows. To deplete $CD25^+$ cells, cells were incubated for 10 min with anti-CD25-PE
458 (PC61), washed in MACS buffer, and incubated for an additional 10 min with anti-PE MACS microbeads
459 (Miltenyi Biotec, Bergisch Gladbach) then subjected to autoMACS purification (Miltenyi Biotec). The
460 negative fraction was used as CD25-depleted spleen cells. A typical depletion resulted in <1% of the $CD4^+$
461 cells expressing CD25. Prior to injection, all cells were washed twice in PBS. Naive TxA23.Thy-1.1 T cells
462 that were isolated from thymus, were mixed into the BALB/c Thy1.2 splenocyte population such that an
463 i.p. injection of 0.3 ml/mouse resulted in the transfer of 100,000 TxA23.Thy-1.1 T cells and 20×10^6 spleen
464 cells. Mice were monitored weekly and euthanized at ~ day 62 for tissue analyses.

465 **Histopathology**

466 BALB/c *nu/nu* mice were euthanized 62 days after receiving an adoptive transfer of splenocytes and naïve
467 $CD4^+$ T cells from autoreactive mice. The stomach opened, washed with cold PBS, and fixed in 4% neutral
468 buffered formalin. Fixed tissues were embedded in paraffin, stained with hematoxylin and eosin (H&E) by
469 Saint Louis University Research Histology Facility (SLU ASBRH) and disease pathology was scored
470 similarly to previously published assessments (*38*). Briefly multiple pathological features, including
471 inflammation, glandular atrophy, and epithelial hyperplasia were graded on a scale of 1–4, depending on
472 the extent of mononuclear cell infiltration and parietal and chief cell destruction. All stomach sections were
473 scored blindly by at least two individuals. General descriptions for scores are as follows: 0, healthy tissue
474 with no abnormalities 0.5, scattered lymphocytes throughout submucosa and muscularis with one or two
475 small dense blankets of lymphocytes; 1, two to four small dense clusters of lymphocytes in the
476 submucosa/mucosa; 1.5, two or three areas with intermediate infiltration spanning one-third of mucosa; 2,
477 big nodules of lymphocytic accumulation spanning half to all of mucosa; 2.5, big nodules of lymphocytic
478 accumulation spanning half to all of mucosa beginning to show evidence of parietal and chief cell
479 destruction (<25%); 3.0, heavy lymphocytic infiltration throughout mucosa, parietal and chief cell loss (25–
480 75%), and replacement by foamy cells; and 4.0, total parietal and chief cell loss, no mucosal architecture,
481 and many foamy cells.

482

483 **Flow Cytometry**

484 Immune cells were isolated from gastric mucosa, gastric/pancreatic or inguinal lymph nodes, and spleens
485 following the protocol previously described and cell surface staining was performed according to standard
486 procedures (*38, 43*). Immune cell subsets and proteins expressed on Tregs were identified using the
487 following antibodies: CD4 BV421, CD8 BV510, CD90.2 BV786, CD4 BV711, CD38 BV711, CD137
488 BV650 CD152 (CTLA4), CD103 PE-Cy7, CD8 PE, CD19 PE (BD Biosciences, Franklin Lakes, New
489 Jersey), CD73 PE/Dazzle594, CD90.1, CD134 PerCP/Cyanine 5.5, Ki67 BV605 (BioLegend, San Diego,
490 California), CD25 APC-eFluor780, Foxp3 APC, CD62L eFlour450, CD44 APC-eFlour780 (Thermo

491 Fisher Scientific). Cells were washed with 200 uL of PBS and stained in only PBS at 4°C. Cells were
492 fixed and permeabilized using eBioscience Foxp3/Transcription Factor Staining Buffer Set (Thermo
493 Fisher Scientific). Cells were incubated overnight with the intracellular antibodies and then washed and
494 analyzed by flow cytometry. Flow cytometry was performed on a BD LSRII, a BD Fortessa (BD
495 Biosciences), or a Cytek Aurora (Cytek Biosciences, Fremont California), and analyzed using FlowJo
496 (FlowJo, Ashland, OR).
497
498 **Single-Cell RNA-seq**
499 Cells from gastric lymph nodes and spleens (day 7 post transfer; day 6 post-treatment) were prepared as
500 above, RBC depleted as needed and filtered through 40µm strainers. Viability (>85%) was confirmed by
501 trypan blue. Cells were loaded on a 10x Genomics Chromium Controller (10X Genomics, Pleasanton,
502 CA) targeting up to 10,000 cells per library using the Next GEM Single Cell 5′ Kit v2 (10x #1000263).
503 cDNA amplification and library prep followed manufacturer protocols. PCR reactions were conducted in
504 the T100 Thermal Cycler (BioRad, Hercules, CA). Libraries were QC'd on an Agilent 2100 Bioanalyzer
505 (Agilent, Santa Clara, CA) and sequenced on an Illumina NovaSeq 6000 (Illumina, San Diego, CA).
506 Raw data were processed through CellRanger 6.0.2 pipeline (10x Genomics). Conditional repeats were
507 combined using cellranger aggr. Analysis was conducted using Seurat. (*44*) Each dataset was filtered to
508 exclude cells with low gene expression (<500/cell), high gene counts (outliers), and high percent
509 mitochondrial transcript load (>10%/cell). Datasets were merged, normalized, scaled, and dimensionally
510 reduced. Layers were joined and clusters were generated using a resolution of 2. Cluster identities were
511 established by attaining distinguishing genes per cluster and relating them to known profiles for immune
512 cells present in spleen and gastric lymph nodes. T cells clusters were subset and pathway analysis was
513 conducted using the R package enrichR and the Msig database for transcripts. Gene ontology, pathway
514 enrichment, and signature analyses (e.g., IL2/STAT5 signaling) were conducted
515 using fgsea and enrichR with MSigDB gene sets. Visualization of feature plots was performed using the
516 ggplot2 package in combination with the scCustomize package. Heatmaps were generated using Seurat's

517 DoHeatMap function. Statistical analyses were performed in Prism 10.0.0 (GraphPad Software). *P* values
518 less than 0.05 were considered significant.
519
520 **Statistical Analysis**
521 In vitro data are expressed as means of individual determination ± SD. In vivo data are expressed as median
522 of individual determination ± 95% confidence interval. Statistical analysis was performed using GraphPad
523 Prism 10 (GraphPad Software, San Diego, CA). Dose titrations of CUE-401 on nTregs utilized Kruskal-
524 Wallis test. Cytokine analysis utilized Wilcoxon matched-pairs signed rank test. In vitro treatment
525 comparisons between rhIL-2, rhIL-2 + TGF-β, and CUE-401 utilized Ordinary one-way ANOVA with
526 Tukey's multiple comparisons test. Histopathology score significance was performed using the Mann–
527 Whitney *U* test. Differential expression analysis between CUE-401 and PBS treated Tregs in scRNA-seq
528 data was performed using the Wilcoxon rank-sum test implemented in Seurat. Differentially expressed
529 genes were identified using the FindMarkers function in the Seurat package with default statistical
530 parameters, a log fold-change threshold of 0.6, and a minimum expression fraction of 0.1. Genes with an
531 adjusted p-value < 0.05 were considered differentially expressed. For bulk RNA sequencing, P-values were
532 adjusted for multiple comparisons using the Benjamini–Hochberg method to control false discovery rate.
533
534 **Figures**:
535

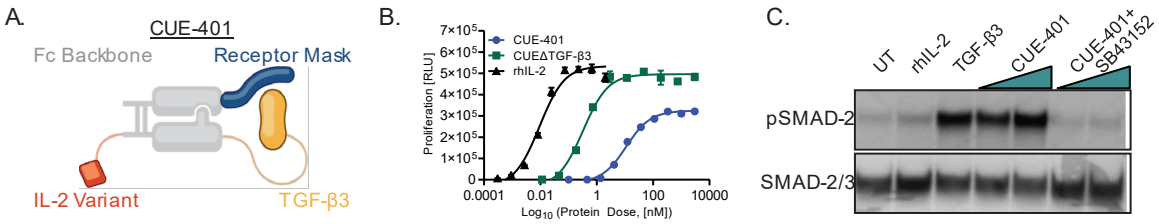

536 **Fig. 1. CUE-401 promotes IL-2 and TGF-β signaling activity.**
537 (**A**) Model of CUE-401 design. (**B**) CTLL-2 proliferation with recombinant human IL-2 (Proleukin),
538 CUE-401, or CUE-401ΔTGF-β3. (**C**) Immunoblot detecting phosphorylated SMAD-2 (pSMAD-2) and

539 total SMAD-2/3 after 30 minutes of stimulation with rhIL-2, rhTGF-β3, CUE-401, or CUE-401 +

540 SB43152.

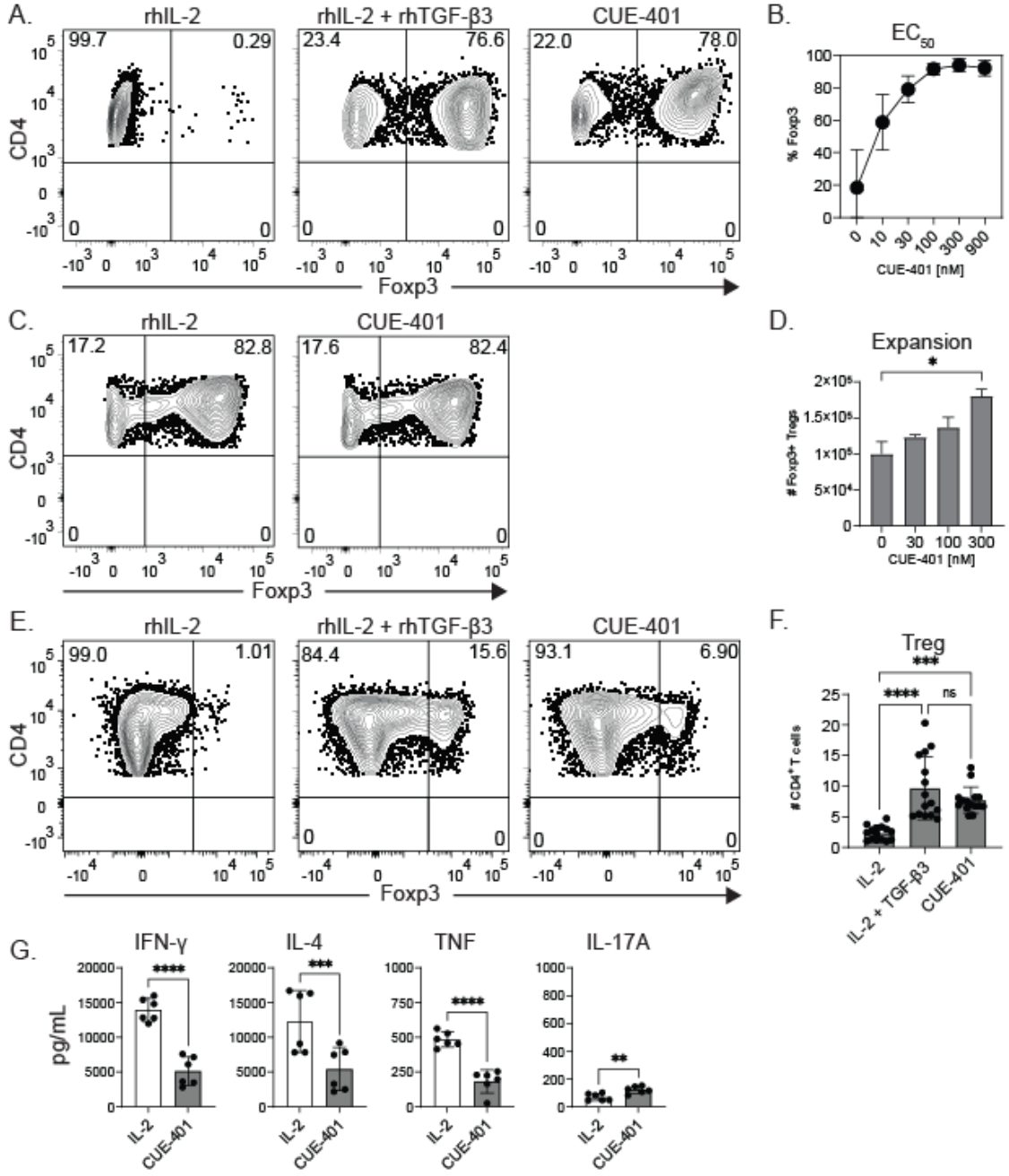

541

542

543 **Fig. 2. CUE-401 promotes iTreg induction, nTreg expansion, and Teff suppression**

544 (**A**). Representative flow cytometric analysis showing the percentage of $CD4^+$ gated cells expressing

545 Foxp3 in vitro following stimulation with rhIL-2, rhIL-2 + rhTGF-β3, or CUE-401. (**B**). Dose-response

546 curve displaying Foxp3 expression with increasing doses of CUE-401. (**C**). Representative flow
547 cytometric analysis showing the percentage of $CD4^+$ gated cells expressing Foxp3 after six days in vitro
548 stimulation of Tregs with rhIL-2 or CUE-401. (**D**). Number of Foxp3 expressing cells at various
549 concentrations of CUE-401. (**E**). Flow cytometric analysis displaying the percentage of $CD4^+$ gated cells
550 expressing Foxp3 after six days in vitro simulation of Teff with rhIL-2, rhIL-2 + rhTGF-β3, or CUE-401.
551 (**F**) Percentages of $CD4^+Foxp3^+$ Tregs in rhIL-2, rhIL-2 + rhTGF-β3 and CUE-401 treated samples. (**G**).
552 Amounts of IFN-γ, IL-4, TNF, and IL-17A secreted from $CD4^+CD44^{hi}$ Foxp3.GFP^- T cells with rhIL-2 or
553 CUE-401 treatment. Flow cytometry plots are representative of individual sorted samples analyzed from
554 thymus (A) or spleen (D,F,G) of 4-8 healthy BALB/c mice. EC_{50} calculated by taking the concentration
555 halfway between the top and bottom value (approximately 20-80%). Bars in each graph represent the
556 mean +/-SD. *P*-values calculated using Kruskal-Wallis test (D), ordinary one-way ANOVA with Tukey's
557 multiple comparisons test (F), or Wilcoxon matched-pairs signed rank test (G) with $*p = 0.0332$, $**p =$
558 0.0021, $***p = 0.0002$, and $****p < 0.0001$.
559
560

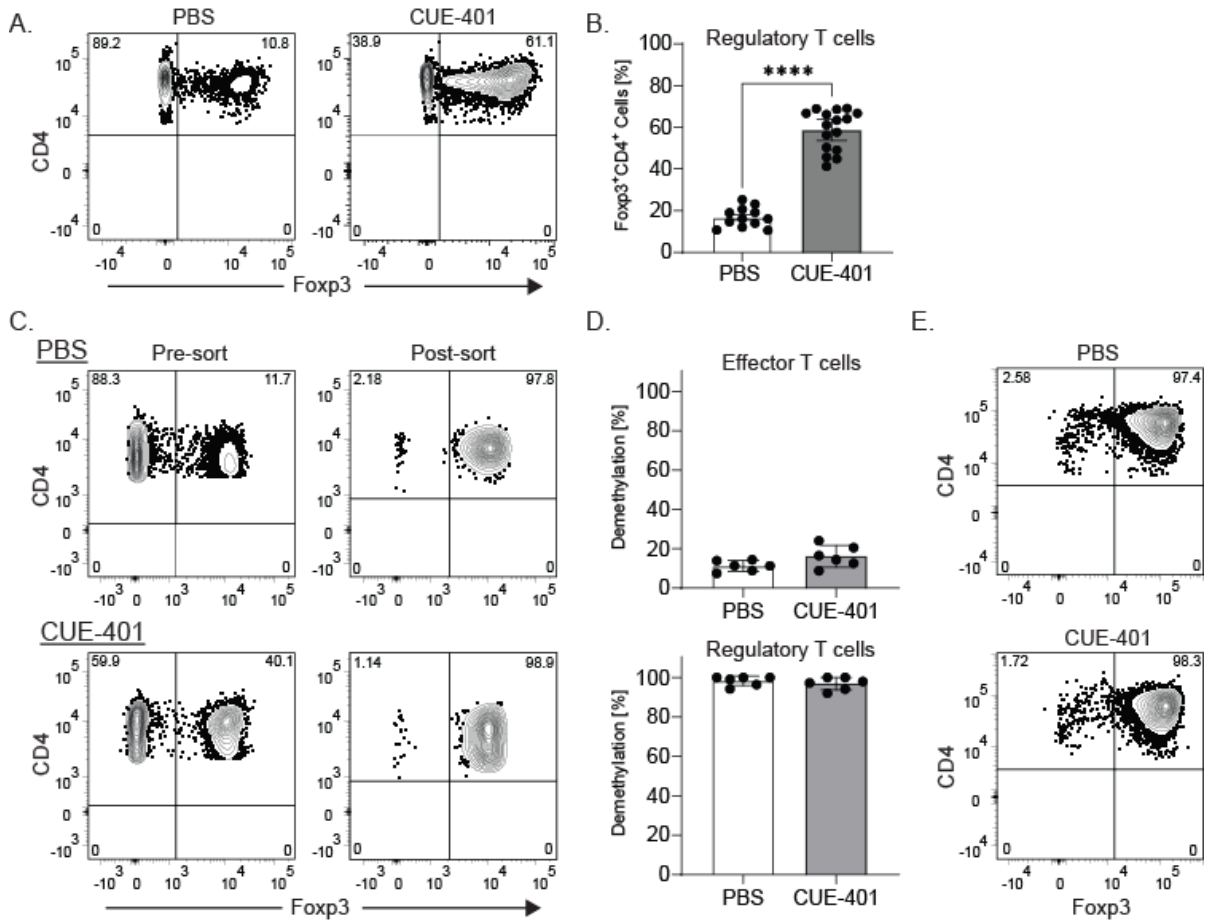

Fig. 3. CUE-401 treatment increases proportions of stable Foxp3+ Tregs in vivo

(**A**) Flow cytometric analysis showing percentages of $CD4^+$ gated cells expressing Foxp3 six days after treatment of BALB/c mice. (**B**) Combined data for the percentages of $CD4^+Foxp3^+$ Tregs in PBS and CUE-401 treated mice. (**C**) Flow cytometric analysis of $CD4^+Foxp3^+$ expression prior to and after performing FACS to purify $CD4^+Foxp3^+GFP^+$ Tregs. (**D**) Results of qPCR quantifying the relative percentage of DNA demethylation at key CpG sites within the Treg-specific demethylated region (TSDR) of the *Foxp3* locus of $CD4^+$Foxp3.eGFP$^-$ and $CD4^+$Foxp3.eGFP$^+$ cells sorted from PBS and CUE-401 treated mice. (**E**) Representative flow cytometric plots showing Foxp3 expression of purified T cells from PBS and CUE-401 treated mice after 6 days of restimulation in vitro in the absence of cytokines. For all graphs, controls were PBS treated age-matched mice. Data in (A-B) was generated from spleens of 2-5 mice in 7 independent experiments. Plots in (C) show the average proportion of $Foxp3^+$ T cells pre and post sorting from 8 mice in 2 independent experiments. Bars represent the median +/- 95% C.I. TSDR

analysis in (D) includes 12 mice from 2 independent experiments. Female mice methylation status was normalized for methylation state on both x chromosomes. *P* values were calculated utilizing the Mann-Whitney *U* test. ****$p < 0.001$.

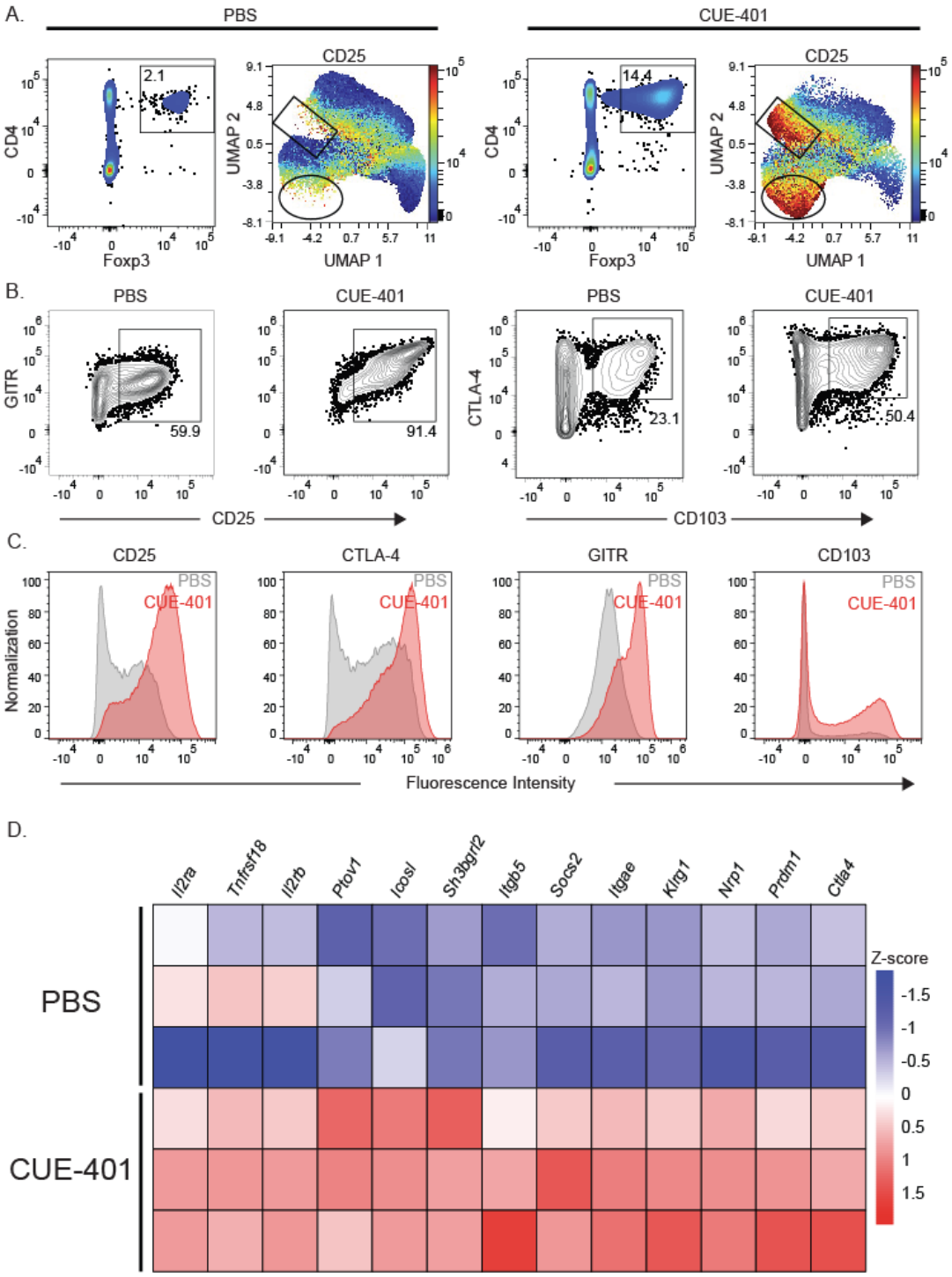

580 **Fig. 4. CUE-401 increases expression of transcripts and proteins associated with Treg activation.**
581 (**A**). Flow cytometric analysis shows the percentage of $CD4^+Foxp3^+$ expressing cells following treatment
582 of mice with PBS or CUE-401. $CD4^+Foxp3^+$ Tregs were identified, and UMAP projections were
583 generated using OMIQ software to cluster cells based on protein expression. The feature plot shows
584 CD25 expression within the $Foxp3^+$ populations. (**B**). Cells were gated on the $CD4^+Foxp3^+$ populations to
585 assess surface expression of GITR, CD25, CTLA-4 and CD103. (**C**). Histograms display the expression
586 of GITR, CD25, CTLA-4, and CD103 within the Treg compartment of PBS-treated controls compared to
587 CUE-401–treated mice. (**D**). Heatmap from bulk RNA sequencing of sorted Tregs, highlighting
588 differentially expressed genes between PBS and CUE-401 treated mice. Genes included had a $\log_2$ fold
589 change > 2 and adjusted p-value < 0.05, using the Benjamini–Hochberg correction to control false
590 discovery rate (FDR). For all flow cytometry plots, data are representative of individual spleens from a
591 single experiment with 3 mice per treatment group. PBS-treated, age-matched mice served as controls in
592 all analyses.

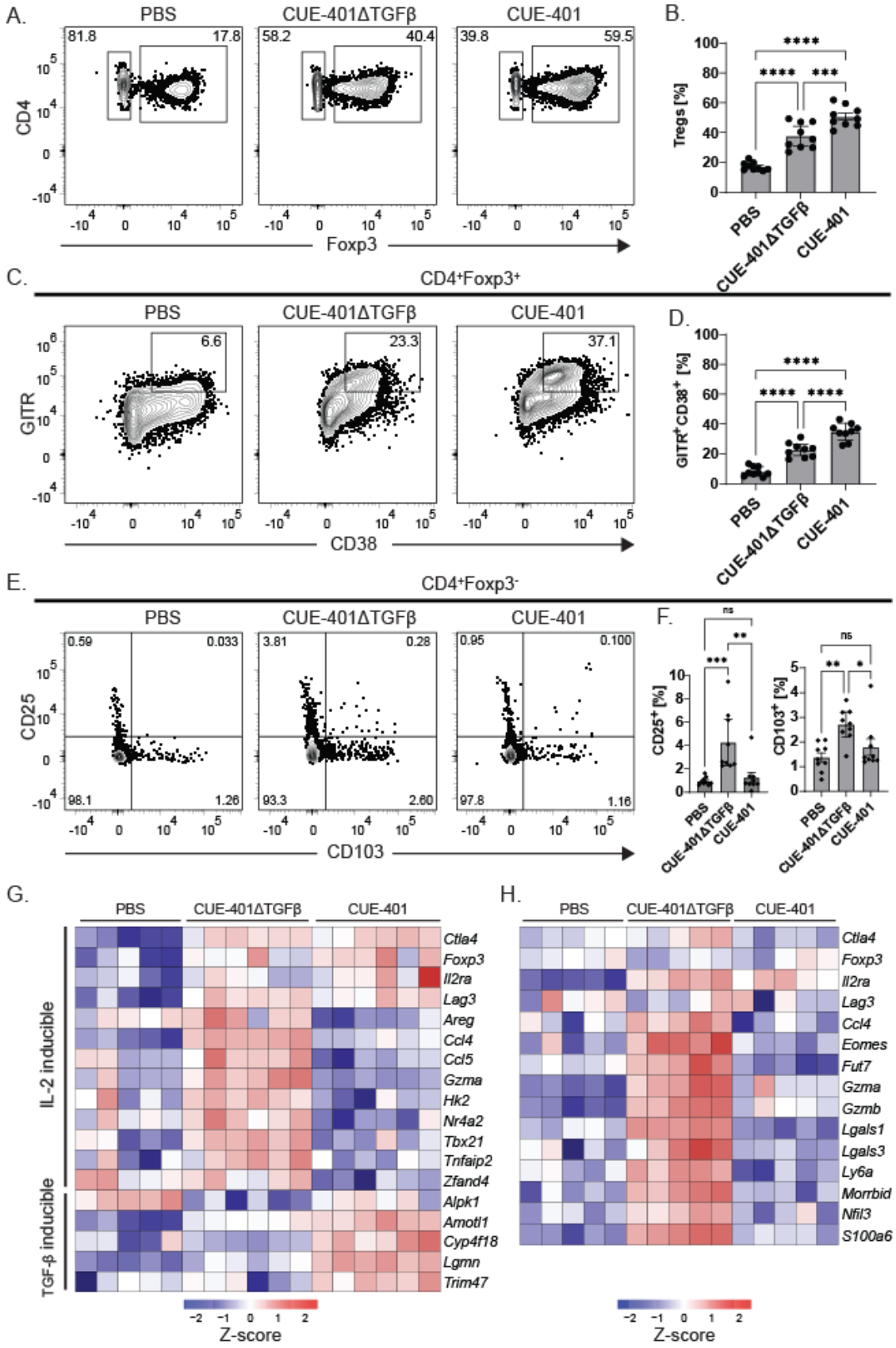
A.
PBS
CUE-401ΔTGFβ
CUE-401
81.8
17.8
58.2
40.4
39.8
59.5
CD4
Foxp3
B.
Tregs [%]
PBS
CUE-401ΔTGFβ
CUE-401
C.
CD4+Foxp3+
6.6
23.3
37.1
GITR
CD38
D.
GITR+CD38+ [%]
E.
CD4+Foxp3-
0.59
0.033
98.1
1.26
3.81
0.28
93.3
2.60
0.95
0.100
97.8
1.16
CD25
CD103
F.
CD25+ [%]
CD103+ [%]
ns
G.
H.
IL-2 inducible
TGF-β inducible
Ctla4
Foxp3
Il2ra
Lag3
Areg
Ccl4
Ccl5
Gzma
Hk2
Nr4a2
Tbx21
Tnfaip2
Zfand4
Alpk1
Amotl1
Cyp4f18
Lgmn
Trim47
Ccl4
Eomes
Fut7
Gzmb
Lgals1
Lgals3
Ly6a
Morrbid
Nfil3
S100a6
Z-score

593

594 **Fig. 5. The combined effects of IL-2 and TGF-β3 in CUE-401 differ from IL-2 treatment alone.**
595 (**A**). Representative flow cytometric analysis showing the percentage of $CD4^+$ gated cells expressing
596 Foxp3 six days after treatment with PBS (left), CUE-401ΔTGF-β3 (middle), or CUE-401 (right) in vivo.
597 (**B**). Combined data showing the percentages of $CD4^+Foxp3^+$ Tregs in PBS, CUE-401ΔTGF-β3, or CUE-
598 401 treated mice. (**C**). Representative flow cytometric analysis comparing GITR by CD38 expression in
599 $CD4^+Foxp3^+$ Tregs following the indicated treatments. (**D**). Combined data showing the percentage of
600 $GITR^+CD38^+$ Tregs following PBS, CUE-401ΔTGF-β3, or CUE-401 treatment. (**E**). Representative flow
601 cytometric analysis comparing CD25 by CD103 of $CD4^+Foxp3^-$ gated cells. (**F**). Combined data showing
602 the percentage of $CD25^+CD4^+Foxp3^-$ cells and $CD103^+CD4^+Foxp3^-$ cells six days after treatment. Data
603 shown are representative of two independent experiments (N = 9 per group). Bars represent the median ±
604 95% confidence interval. (**G**, **H**). Heatmaps of gene expression profiles in sorted $CD4^+Foxp3.eGFP^+$
605 Treg cells or $CD4^+Foxp3.eGFP^-$ Tconv cells, derived from a subset of control or treated mice (N = 2,3 per
606 group, respectively). *P* values for flow results were determined utilizing an ordinary one-way ANOVA
607 with Tukey's multiple comparisons test with $*p = 0.0332$, $**p = 0.0021$, $***\ p = 0.0002$, and $****p <$
608 0.0001.
609
610

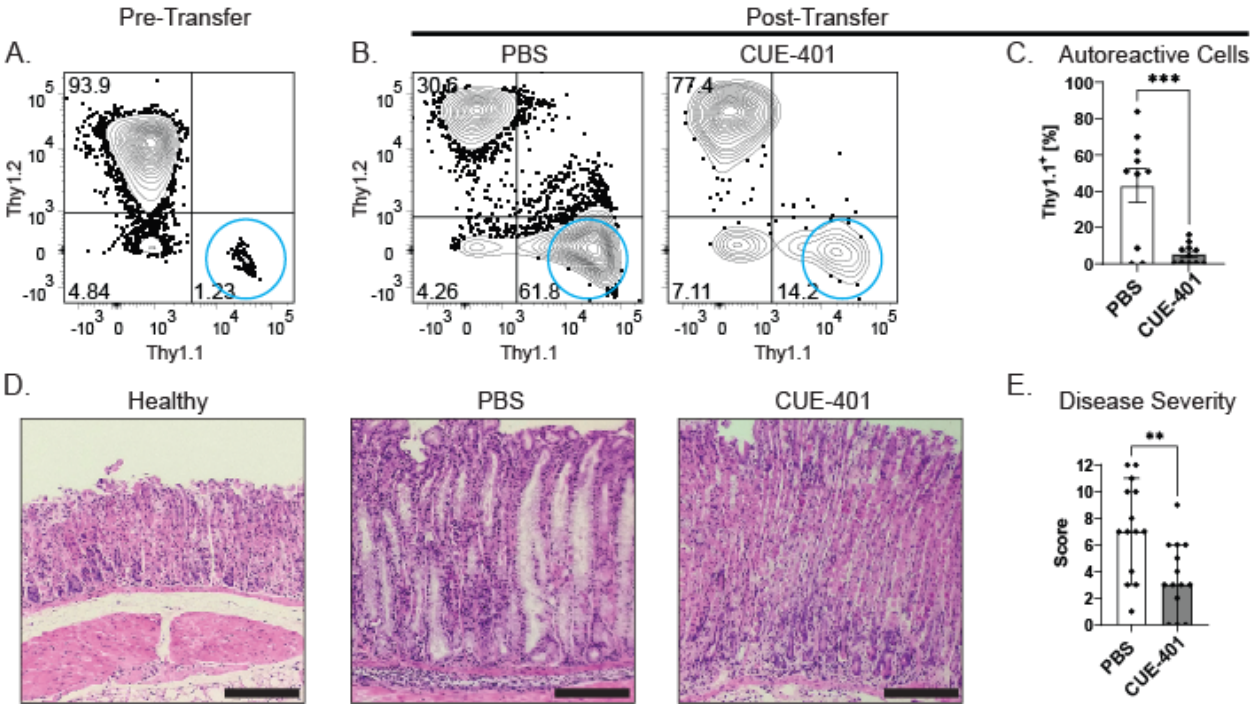

611

612 **Fig. 6. CUE-401 treatment inhibits Teff responses and decreases autoimmune disease severity.**

613 (**A**). Flow cytometric analysis of Thy1.2^{+}CD4^{+} splenocytes and autoreactive Thy1.1^{+}CD4^{+} splenocytes

614 prior to injection into BALB/c *nu/nu* mice. (**B**). Flow cytometric analysis of Thy1.1 and Thy1.2

615 expression in CD4^{+} T cells from stomachs of BALB/c *nu/nu* mice ~62 days after transfer. (**C**) Combined

616 analysis of Thy1.1 expressing autoreactive cells in the gastric mucosa of nude mice ~62 days after

617 transfer and subsequent treatment with PBS or CUE-401. Quantified data are presented as mean ± SEM.

618 Experiments were conducted independently three times, with 2–5 mice per group per experiment. (**D**).

619 Representative images from four independent experiments, comparing tissues from healthy untreated

620 BALB/c mice, PBS-treated BALB/c *nu/nu* controls, and CUE-401–treated BALB/c *nu/nu* mice. (**E**).

621 Histological disease scores were determined based on multiple pathological features, including

622 inflammation, glandular atrophy, and epithelial hyperplasia. The final score represents the combined

623 values from these categories. Graph bars represent the median +/- 95% C.I. Experiments contained 3-5

624 aged matched female mice. *P*-values were determined utilizing either Unpaired Student's T test (C) or

625 Mann-Whitney *U* test (D) with $^{**}p = 0.0040$ and $^{***}p = 0.0005$. Scale bars in micrographs represent 180

626 μM.

627

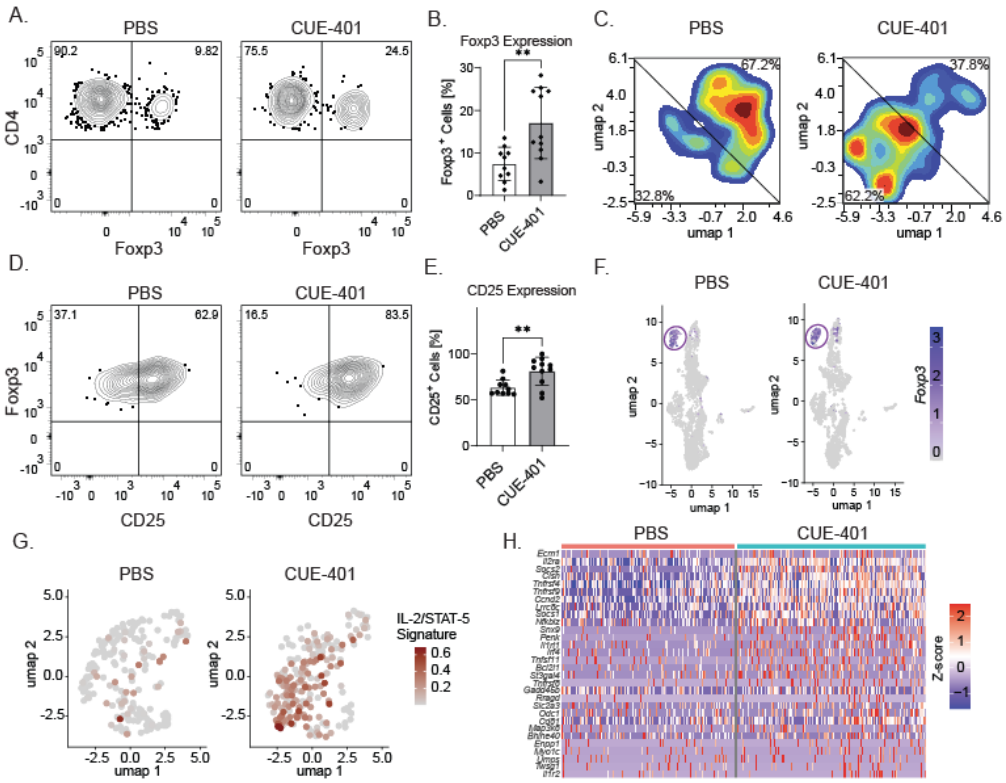

628

629 **Fig. 7. CUE-401 induces activated Tregs with a distinct transcriptional program.**

630 (**A**). Representative flow cytometric analysis of CD4 gated Foxp3^{+} cells in PBS and CUE-401 treated

631 BALB/c nude mice 7 days after splenocyte transfer. (**B**). Cumulative data showing the percentages of

632 CD4^{+}Foxp3^{+} Tregs in PBS and CUE-401 treated mice 6 days after a single treatment. (**C**). CD4^{+}Foxp3^{+}

633 Tregs were identified in each treatment condition, and UMAP projections generated distinct clusters of

634 cells based on protein expression. (**D**). Representative flow cytometric analysis of CD4^{+}Foxp3^{+} gated,

635 CD25 expressing cells. (**E**). Combined data showing the percentages of CD25 expressing Tregs in PBS

636 and CUE-401 treated mice. (**F**). Single cell RNA sequencing clustering analysis of T cells. T cell

637 populations were subset and Foxp3 expression identified the Treg populations in PBS and CUE-401

638 treated mice. (**G**). Foxp3 expressing T cells were re-clustered and signatures were generated based on IL-

639 2/STAT5 signaling transcripts that were identified through gene set enrichment analysis

640 (**H**). Heatmap that highlights differentially expressed genes in single Foxp3^{+} cells between PBS and CUE-

641 401 treatment. Differential expression analysis between CUE-401 and PBS Tregs used the Wilcoxon

642 rank-sum test implemented in Seurat. P-values were adjusted for multiple comparisons using the
643 Benjamini–Hochberg method to control false discovery rate (FDR). Representative images in (A) from 3
644 independent experiments with 3-5 age matched female mice per experiment. *P*-values were determined
645 utilizing Mann-Whitney *U* test with $p < 0.05$ as significant for the flow cytometry analyses. Single cell
646 analysis in (F-H) generated cells of 8 total mice in 2 independent experiments (4 treated and 4 untreated).
647

648 **Acknowledgments:**

649 We thank Saint Louis University Flow Cytometry Core (Joy Eslick, and Jacqueline Spencer) and the
650 Advanced Research Histology Facility (Caroline Murphy, Vasiliki Grammatopoulou) for assistance with
651 data collection. We thank Saint Louis University Genomics and Bioinformatics Core Facility (Dr.
652 Michelle Brennan) for assistance with processing and analysis of single cell and bulk RNA sequencing.
653 We thank Saint Louis University Department of Comparative Medicine (Lisa Tempel, Tawanika
654 Williams, Kelsey Ernst) for assistance in animal care and handling

655

656 **Funding:**

657 This work was funded in part by a sponsored research agreement between CUE Biopharma and Saint
658 Louis University.

659

660 **Author contributions:**

661 Conceptualization: NMJ, RS, NMG, SNQ, AS, CAP, SGH, EF, RJD

662 Methodology: NMJ, NMG, SNQ, RJD, SL, EC, KY, EN

663 Investigation: NMJ

664 Visualization: NMJ, KF, JAC, RJD

Formal Analysis: NMJ, NY, CAP, SGH, KF, EF

Software: SGH, KF

Funding acquisition: AS, NMG, SNQ, RJD

Writing – original draft: NMJ, JAC, RJD

Writing – review & editing: NMJ, JAC, NMG, SNQ, RJD

All authors approved the final manuscript.

Competing interests: AS, SL, NMG, SNQ, RS, KY, EN, and EC are employees of CUE Biopharma. All other authors declare that they have no competing interests.

Data and materials availability: All data necessary to understand and evaluate the conclusions of the paper are provided in the manuscript and supplementary materials. The CUE-401 biologic can be available upon request under a material transfer agreement with CUE Biopharma. Sequencing data will be made publicly available upon acceptance of this publication.

687 **References:**

688 1. S. Sakaguchi, N. Sakaguchi, M. Asano, M. Itoh, M. Toda, Immunologic self-tolerance maintained by
689 activated T cells expressing IL-2 receptor alpha-chains (CD25). Breakdown of a single mechanism of self-
690 tolerance causes various autoimmune diseases. *J Immunol* **155**, 1151-1164 (1995).
691 2. L. Wang *et al.*, Regulatory T cells in homeostasis and disease: molecular mechanisms and therapeutic
692 potential. *Signal Transduct Target Ther* **10**, 345 (2025).
693 3. C. L. Bennett *et al.*, The immune dysregulation, polyendocrinopathy, enteropathy, X-linked syndrome
694 (IPEX) is caused by mutations of FOXP3. *Nat Genet* **27**, 20-21 (2001).
695 4. S. Hori, T. Nomura, S. Sakaguchi, Control of regulatory T cell development by the transcription factor
696 Foxp3. *Science* **299**, 1057-1061 (2003).
697 5. R. Khattri, T. Cox, S. A. Yasayko, F. Ramsdell, An essential role for Scurfin in CD4+CD25+ T regulatory
698 cells. *Nat Immunol* **4**, 337-342 (2003).
699 6. J. D. Fontenot, M. A. Gavin, A. Y. Rudensky, Foxp3 programs the development and function of
700 CD4+CD25+ regulatory T cells. *Nat Immunol* **4**, 330-336 (2003).
701 7. E. M. Shevach, A. M. Thornton, tTregs, pTregs, and iTregs: similarities and differences. *Immunol Rev* **259**,
702 88-102 (2014).
703 8. A. Jones, D. Hawiger, Peripherally Induced Regulatory T Cells: Recruited Protectors of the Central
704 Nervous System against Autoimmune Neuroinflammation. *Front Immunol* **8**, 532 (2017).
705 9. T. S. Davidson, R. J. DiPaolo, J. Andersson, E. M. Shevach, Cutting Edge: IL-2 is essential for TGF-beta-
706 mediated induction of Foxp3+ T regulatory cells. *J Immunol* **178**, 4022-4026 (2007).
707 10. W. Chen *et al.*, Conversion of peripheral CD4+CD25- naive T cells to CD4+CD25+ regulatory T cells by
708 TGF-beta induction of transcription factor Foxp3. *J Exp Med* **198**, 1875-1886 (2003).
709 11. T. L. Nguyen, N. T. Makhlouf, B. A. Anthony, R. M. Teague, R. J. DiPaolo, In vitro induced regulatory T
710 cells are unique from endogenous regulatory T cells and effective at suppressing late stages of ongoing
711 autoimmunity. *PLoS One* **9**, e104698 (2014).
712 12. S. E. Weber *et al.*, Adaptive islet-specific regulatory CD4 T cells control autoimmune diabetes and mediate
713 the disappearance of pathogenic Th1 cells in vivo. *J Immunol* **176**, 4730-4739 (2006).
714 13. R. J. DiPaolo *et al.*, Autoantigen-specific TGFbeta-induced Foxp3+ regulatory T cells prevent
715 autoimmunity by inhibiting dendritic cells from activating autoreactive T cells. *J Immunol* **179**, 4685-4693
716 (2007).
717 14. S. G. Zheng *et al.*, CD4+ and CD8+ regulatory T cells generated ex vivo with IL-2 and TGF-beta suppress
718 a stimulatory graft-versus-host disease with a lupus-like syndrome. *J Immunol* **172**, 1531-1539 (2004).
719 15. M. E. Raeber, D. Sahin, U. Karakus, O. Boyman, A systematic review of interleukin-2-based
720 immunotherapies in clinical trials for cancer and autoimmune diseases. *EBioMedicine* **90**, 104539 (2023).
721 16. R. Zhang *et al.*, Low-dose IL-2 therapy in autoimmune diseases: An update review. *Int Rev Immunol* **43**,
722 113-137 (2024).
723 17. L. Khoryati *et al.*, An IL-2 mutein engineered to promote expansion of regulatory T cells arrests ongoing
724 autoimmunity in mice. *Sci Immunol* **5**, (2020).
725 18. S. N. Quayle *et al.*, CUE-101, a Novel E7-pHLA-IL2-Fc Fusion Protein, Enhances Tumor Antigen-
726 Specific T-Cell Activation for the Treatment of HPV16-Driven Malignancies. *Clin Cancer Res* **26**, 1953-
727 1964 (2020).
728 19. D. J. Stauber, E. W. Debler, P. A. Horton, K. A. Smith, I. A. Wilson, Crystal structure of the IL-2 signaling
729 complex: paradigm for a heterotrimeric cytokine receptor. *Proc Natl Acad Sci U S A* **103**, 2788-2793
730 (2006).
731 20. K. M. Heaton, G. Ju, E. A. Grimm, Human interleukin 2 analogues that preferentially bind the
732 intermediate-affinity interleukin 2 receptor lead to reduced secondary cytokine secretion: implications for
733 the use of these interleukin 2 analogues in cancer immunotherapy. *Cancer Res* **53**, 2597-2602 (1993).
734 21. T. R. Mosmann *et al.*, Species-specificity of T cell stimulating activities of IL 2 and BSF-1 (IL 4):
735 comparison of normal and recombinant, mouse and human IL 2 and BSF-1 (IL 4). *J Immunol* **138**, 1813-
736 1816 (1987).
737 22. K. Abnaof *et al.*, TGF-beta stimulation in human and murine cells reveals commonly affected biological
738 processes and pathways at transcription level. *BMC Syst Biol* **8**, 55 (2014).
739 23. J. E. Zuniga *et al.*, Assembly of TbetaRI:TbetaRII:TGFbeta ternary complex in vitro with receptor
740 extracellular domains is cooperative and isoform-dependent. *J Mol Biol* **354**, 1052-1068 (2005).

741 24. J. Groppe *et al.*, Cooperative assembly of TGF-beta superfamily signaling complexes is mediated by two
742 disparate mechanisms and distinct modes of receptor binding. *Mol Cell* **29**, 157-168 (2008).
743 25. X. Li, Y. Liang, M. LeBlanc, C. Benner, Y. Zheng, Function of a Foxp3 cis-element in protecting
744 regulatory T cell identity. *Cell* **158**, 734-748 (2014).
745 26. A. S. Wegrzyn, A. E. Kedzierska, A. Obojski, Identification and classification of distinct surface markers
746 of T regulatory cells. *Front Immunol* **13**, 1055805 (2022).
747 27. C. Gootjes, J. J. Zwaginga, B. O. Roep, T. Nikolic, Defining Human Regulatory T Cells beyond FOXP3:
748 The Need to Combine Phenotype with Function. *Cells* **13**, (2024).
749 28. S. Dikiy, A. Y. Rudensky, Principles of regulatory T cell function. *Immunity* **56**, 240-255 (2023).
750 29. J. D. Fontenot, J. P. Rasmussen, M. A. Gavin, A. Y. Rudensky, A function for interleukin 2 in Foxp3-
751 expressing regulatory T cells. *Nat Immunol* **6**, 1142-1151 (2005).
752 30. A. Arvey *et al.*, Inflammation-induced repression of chromatin bound by the transcription factor Foxp3 in
753 regulatory T cells. *Nat Immunol* **15**, 580-587 (2014).
754 31. J. A. Hill *et al.*, Foxp3 transcription-factor-dependent and -independent regulation of the regulatory T cell
755 transcriptional signature. *Immunity* **27**, 786-800 (2007).
756 32. N. Sugimoto *et al.*, Foxp3-dependent and -independent molecules specific for CD25+CD4+ natural
757 regulatory T cells revealed by DNA microarray analysis. *Int Immunol* **18**, 1197-1209 (2006).
758 33. M. Ahn, J. Dostal, P. Hegde, D. J. Lee, CTLA-4 expression on tregs is needed for suppression of
759 autoimmune uveitis. *Sci Rep* **15**, 17745 (2025).
760 34. M. G. Petrillo *et al.*, GITR+ regulatory T cells in the treatment of autoimmune diseases. *Autoimmun Rev*
761 **14**, 117-126 (2015).
762 35. S. Tagkareli *et al.*, CD103 integrin identifies a high IL-10-producing FoxP3(+) regulatory T-cell population
763 suppressing allergic airway inflammation. *Allergy* **77**, 1150-1164 (2022).
764 36. K. E. Earle *et al.*, In vitro expanded human CD4+CD25+ regulatory T cells suppress effector T cell
765 proliferation. *Clin Immunol* **115**, 3-9 (2005).
766 37. R. S. McHugh, E. M. Shevach, D. H. Margulies, K. Natarajan, A T cell receptor transgenic model of
767 severe, spontaneous organ-specific autoimmunity. *Eur J Immunol* **31**, 2094-2103 (2001).
768 38. R. J. DiPaolo, D. D. Glass, K. E. Bijwaard, E. M. Shevach, CD4+CD25+ T cells prevent the development
769 of organ-specific autoimmune disease by inhibiting the differentiation of autoreactive effector T cells. *J*
770 *Immunol* **175**, 7135-7142 (2005).
771 39. S. Gaggero *et al.*, IL-2 is inactivated by the acidic pH environment of tumors enabling engineering of a pH-
772 selective mutein. *Sci Immunol* **7**, eade5686 (2022).
773 40. W. J. Leonard, J. X. Lin, Strategies to therapeutically modulate cytokine action. *Nat Rev Drug Discov* **22**,
774 827-854 (2023).
775 41. D. A. Horwitz *et al.*, Nanoparticles loaded with IL-2 and TGF-beta promote transplantation tolerance to
776 alloantigen. *Front Immunol* **15**, 1429335 (2024).
777 42. W. Lin *et al.*, Regulatory T cell development in the absence of functional Foxp3. *Nat Immunol* **8**, 359-368
778 (2007).
779 43. F. Alderuccio, B. H. Toh, P. A. Gleeson, I. R. van Driel, A novel method for isolating mononuclear cells
780 from the stomachs of mice with experimental autoimmune gastritis. *Autoimmunity* **21**, 215-221 (1995).
781 44. Y. Hao *et al.*, Dictionary learning for integrative, multimodal and scalable single-cell analysis. *Nat*
782 *Biotechnol* **42**, 293-304 (2024).
783 45. D. Haribhai *et al.*, Regulatory T cells dynamically control the primary immune response to foreign antigen.
784 *J Immunol* **178**, 2961-2972 (2007).
785